

# The efficiency of ionising photon production and the radiation energy balance in compact star-forming galaxies

Y. I. Izotov<sup>1,2,\*</sup>, N. G. Guseva<sup>1,2</sup>, K. J. Fricke<sup>2,3</sup>, C. Henkel<sup>2,4</sup>, & D. Schaerer<sup>5,6</sup>

<sup>1</sup>Main Astronomical Observatory, Ukrainian National Academy of Sciences, 27 Zabolotnoho str., Kyiv 03141, Ukraine

<sup>2</sup>Max-Planck-Institut für Radioastronomie, Auf dem Hügel 69, 53121 Bonn, Germany

<sup>3</sup>Institut für Astrophysik, Göttingen Universität, Friedrich-Hund-Platz 1, 37077 Göttingen, Germany

<sup>4</sup>Astronomy Department, King Abdulaziz University, P.O. Box 80203, Jeddah 21589, Saudi Arabia

<sup>5</sup>Observatoire de Genève, Université de Genève, 51 Ch. des Maillettes, 1290, Versoix, Switzerland

<sup>6</sup>IRAP/CNRS, 14, Av. E. Belin, 31400 Toulouse, France

Accepted XXX. Received YYY; in original form ZZZ

## ABSTRACT

We derive apparent and absolute ultraviolet (UV) magnitudes, and luminosities in the infrared (IR) range of a large sample of low-redshift ( $0 < z < 1$ ) compact star-forming galaxies (CSFGs) selected from the Data Release 12 of the Sloan Digital Sky Survey (SDSS). These data are used to constrain the extinction law in the UV for our galaxies and to compare the absorbed radiation in the UV range with the emission in the IR range. We find that the modelled far- and near-UV apparent magnitudes are in good agreement with the observed *Galaxy Evolution Explorer* (GALEX) magnitudes. It is found that galaxies with low and high equivalent widths  $EW(H\beta)$  of the  $H\beta$  emission line require different reddening laws with steeper slopes for galaxies with higher  $EW(H\beta)$ . This implies an important role of the hard ionising radiation in shaping the dust grain size distribution. The IR emission in the range of 8 – 1000  $\mu\text{m}$  is determined using existing data obtained by various infrared space telescopes. We find that the radiation energy absorbed in the UV range is nearly equal to the energy emitted in the IR range leaving very little room for hidden star formation in our galaxies. Using extinction-corrected  $H\beta$  luminosities and modelled SEDs in the UV range we derive efficiencies of ionising photon production  $\xi$  for the entire sample of CSFGs. It is found that  $\xi$  in CSFGs with high  $EW(H\beta)$  are among the highest known for low- and high-redshift galaxies. If galaxies with similar properties existed at redshifts  $z = 5 - 10$ , they could be considered as promising candidates for the reionisation of the Universe.

**Key words:** galaxies: dwarf — galaxies: fundamental parameters — galaxies: irregular — galaxies: ISM — galaxies: starburst

## 1 INTRODUCTION

Recent studies of low-redshift compact star-forming galaxies (hereafter CSFGs) revealed their important role in understanding star formation (SF) processes in galaxies at various redshifts. Izotov et al. (2016c) have shown that the SF in these galaxies is characterised by strong short bursts. This conclusion is based on the difference of the relations between stellar mass  $M_*$  and  $H\beta$  luminosity  $L(H\beta)$  for CSFGs with high and low equivalent widths  $EW(H\beta)$  of the  $H\beta$  emission line. Assuming bursting SF in CSFGs and correcting the  $L(H\beta)$  for the burst age removes differences of  $M_* - L(H\beta)$  relations for CSFGs with different  $EW(H\beta)$  (compare Figs.

9a and 9b in Izotov et al. 2016c) while the assumption of continuous SF fails to reproduce the data. The validity of a bursting scenario is further supported by a comparison of *Galaxy Evolution Explorer* (GALEX) FUV-to- $H\beta$  and NUV-to- $H\beta$  luminosity ratios for CSFGs with high and low  $EW(H\beta)$ s (compare Figs. 6 and 8 in Izotov et al. 2016c). Subsamples of those low- $z$  CSFGs are “Green Pea” (GP) galaxies at redshifts  $\sim 0.1 - 0.3$  selected by their intense green colour on Sloan Digital Sky Survey (SDSS) composite images (Cardamone et al. 2009) and luminous compact galaxies (LCGs) in a larger redshift range selected using not only photometric but spectroscopic SDSS data as well (Izotov, Guseva & Thuan 2011).

One of the most important features of CSFGs is that they very closely resemble in many respects high-redshift

\* E-mail: izotov@mao.kiev.ua

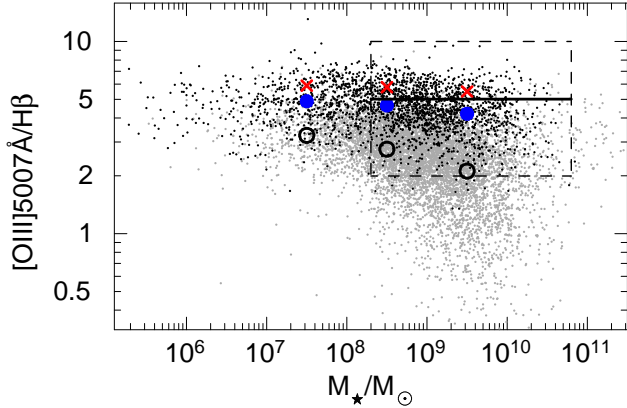


**Figure 1.** The dependence of the  $[\text{O III}]\lambda 5007/\text{H}\beta$  flux ratio on the stellar mass  $M_*$ . Compact SFGs (CSFGs) with  $\text{EW}(\text{H}\beta) \geq 50\text{\AA}$  and  $\text{EW}(\text{H}\beta) < 50\text{\AA}$  are shown by black and grey dots, respectively. The region delineated by a dashed line indicates ranges of  $[\text{O III}]\lambda 5007/\text{H}\beta$  and  $M_*$  for a sample of Lyman-break galaxies (LBGs) at  $z \sim 3.5$  with a median value of  $[\text{O III}]\lambda 5007/\text{H}\beta$  shown by a solid line (Schenker et al. 2013; Troncoso et al. 2014; Holden et al. 2016). Average values of  $[\text{O III}]\lambda 5007/\text{H}\beta$  in 1 dex bins of  $M_*$  are shown by red crosses ( $\text{EW}(\text{H}\beta) \geq 150\text{\AA}$ ), blue filled circles ( $\text{EW}(\text{H}\beta) \geq 50\text{\AA}$ ), and black open circles ( $\text{EW}(\text{H}\beta) < 50\text{\AA}$ ), respectively.

SFGs. In particular, their stellar masses, luminosities, and chemical composition are similar (Izotov et al. 2014a). Low- $z$  CSFGs and high- $z$  SFGs follow the same luminosity-metallicity, stellar mass-metallicity and star-formation rate (SFR) – stellar mass relations (Izotov et al. 2015). Furthermore, strong emission lines are present in the SDSS optical spectra of CSFGs, and their emission in the UV and optical ranges is dominated by the radiation of numerous young massive stars formed during the above mentioned short bursts of star formation (Izotov et al. 2016c).

The importance of studying CSFGs is strengthened by the discovery of the escaping ionising radiation in the Lyman continuum (LyC) in some of these galaxies with high  $[\text{O III}]\lambda 5007/[\text{O II}]\lambda 3727$  emission-line ratios (Izotov et al. 2016a,b). This finding and high efficiency of ionising photon production (Schaerer et al. 2016) support the idea that their counterparts at redshifts  $z \sim 5 - 10$  were likely the main sources of the reionisation of the Universe.

A large sample of CSFGs opens an opportunity to study relations between dust extinction in the UV range and its emission in the infrared (IR) range for the galaxies with various stellar masses, luminosities, and metallicities by means of spectral energy distribution (SED) fitting of the SDSS spectra and their extrapolation to the UV. In particular, Izotov et al. (2016a,b) showed that the extrapolation to the UV range of the SEDs obtained from the optical SDSS spectra reproduces FUV and NUV *HST* Cosmic Origin Spectrograph (COS) spectra reasonably well adopting the Cardelli, Clayton & Mathis (1989) reddening law and the ratio of the absolute-to-selective extinctions  $R(V) = A(V)/E(B - V) < 3.1$ . However, this result was obtained only for five extreme CSFGs, which were observed with the *HST*/COS, and needs to be confirmed on larger samples of CSFGs.

The relations between interstellar extinction, UV and

IR emission in low- and high-redshift SFGs were extensively discussed in the past (e.g. Meurer, Heckman & Calzetti 1999; Calzetti, Kinney & Storchi-Bergmann 1994; Calzetti et al. 2000; Reddy et al. 2010, 2012; Boquien et al. 2012; Forrest et al. 2016; Shivaeei et al. 2016). However, no such study was conducted for large samples of CSFGs. One of the advantages of these galaxies is their compactness, which ensures that aperture corrections needed to adjust spectroscopic and photometric observations are relatively small allowing to combine both sets of data. Thus, different apertures do not introduce biases by comparing optical spectroscopic data with UV and IR photometric data.

The aim of this paper is threefold. First, we study the ability of SED fitting of the SDSS spectra to reproduce the observed apparent magnitudes of our sample galaxies in the UV range. We obtain slopes of the modelled SEDs in the UV range for further comparison with those of other samples consisting of low- and high- $z$  SFGs and to study, which factors determining these slopes are most important, extinction or starburst age. Second, using extinction coefficients and  $\text{H}\beta$  emission-line fluxes obtained from the SDSS spectra we derive the efficiency of ionising photon production of CSFGs, an important parameter in studies of cosmic reionisation. Third, we wish to compare luminosities of the absorbed UV radiation derived from the SED modelling with the luminosities of SFGs in the IR range and to test whether any signs of hidden SF are present in CSFGs. We also wish to derive IR excesses, the ratios of IR and UV luminosities for the entire sample of CSFGs, and to compare them with those for other samples of low- and high- $z$  SFGs.

In Sect. 2 we discuss the sample, modelling of the SEDs and the determination of galaxy integrated parameters. The comparison of the modelled and observed galaxy UV magnitudes and the determination of the most appropriate reddening law is discussed in Sect. 3. We derive the intrinsic and observed SED slopes in the UV range and the efficiency of ionising photon production in Sects. 4 and 5. In Sect. 6 the radiation absorbed in the UV is compared with the radiation emitted in the IR. We derive IR excesses for CSFGs and compare them with those for other samples of low- and high- $z$  SFGs. The main results of the paper are summarised in Sect. 7.

## 2 THE SAMPLE OF CSFGS

A sample of CSFGs was selected from the SDSS Data Release 12 (DR12) (Alam et al. 2015). Selection criteria were described by Izotov et al. (2015). Two main criteria were compactness and stellar origin of ionising radiation. Only galaxies with an angular radius on the SDSS images  $R_{50} \leq 3''$  were selected, where  $R_{50}$  is the galaxy's Petrosian radius within which 50% of the galaxy's flux in the SDSS  $r$  band is contained. Furthermore, all selected galaxies occupy the region of SFGs below the empirical Kauffmann et al. (2003) SFG – AGN dividing line on the emission-line diagram  $[\text{O III}]\lambda 5007/\text{H}\beta - [\text{N I}]\lambda 6584/\text{H}\alpha$  by Baldwin, Phillips & Terlevich (1981). Izotov et al. (2016c) selected  $\sim 14000$  galaxies with redshifts  $z < 1$  using the criteria mentioned above. The BPT diagram of CSFGs is shown in Fig. 1 of Izotov et al. (2016c). All these galaxies are characterised by spectra with narrow emission lines and

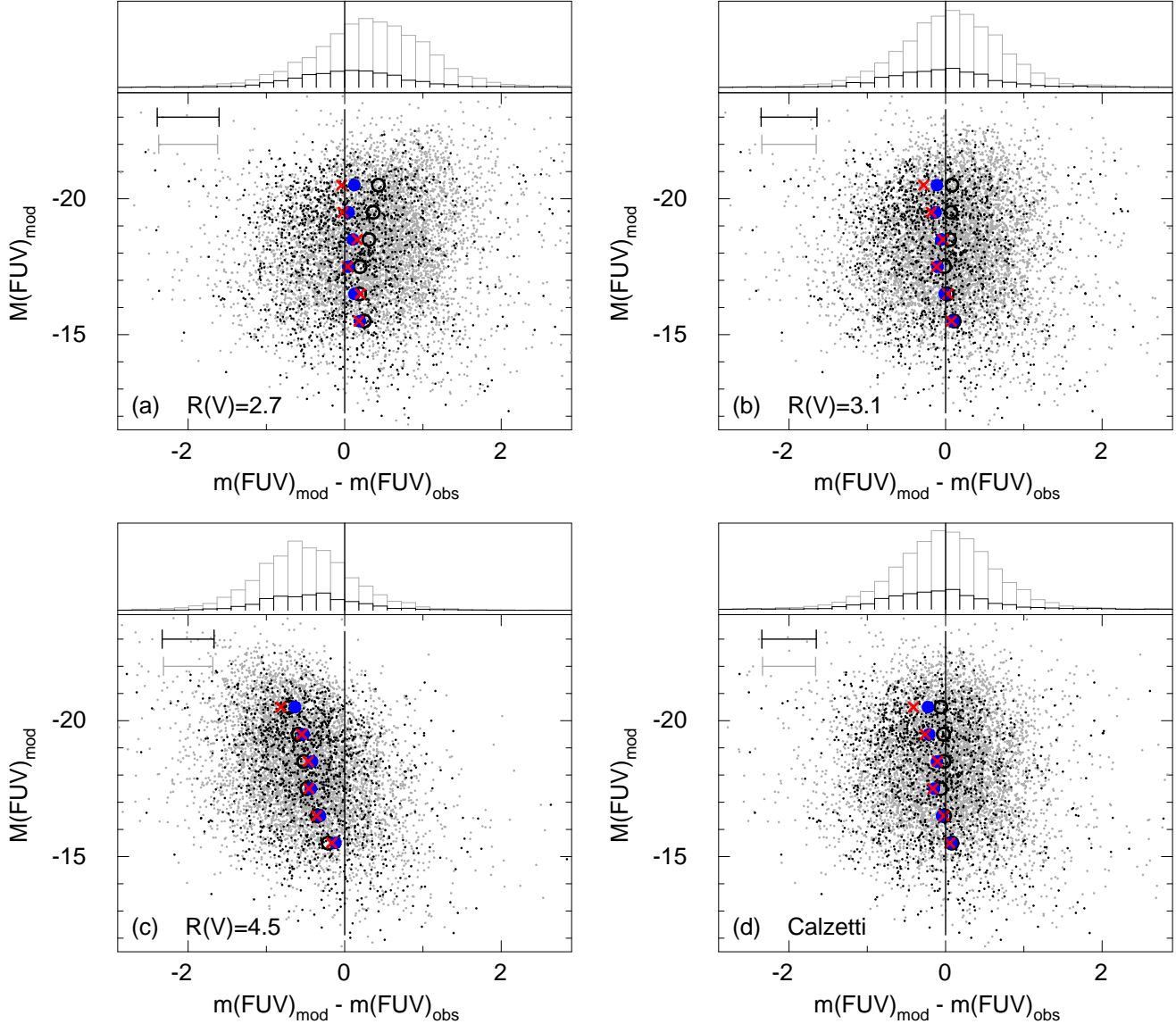


**Figure 2.** The dependence of the difference between modelled and *GALEX* observed apparent FUV magnitudes  $m(\text{FUV})_{\text{mod}} - m(\text{FUV})_{\text{obs}}$  on the modelled rest-frame absolute FUV magnitude  $M(\text{FUV})_{\text{mod}}$  (a-c) adopting the [Cardelli et al. \(1989\)](#) reddening law with various  $R(V)$ s and (d) the [Calzetti et al. \(1994\)](#) reddening law. Galaxies with  $\text{EW}(\text{H}\beta) \geq 50 \text{ \AA}$  and  $< 50 \text{ \AA}$  are shown by black and grey dots, respectively. Average values of  $m(\text{FUV})_{\text{mod}} - m(\text{FUV})_{\text{obs}}$  in 1 mag bins of  $M(\text{FUV})_{\text{mod}}$  are shown by red crosses ( $\text{EW}(\text{H}\beta) \geq 150 \text{ \AA}$ ), blue filled circles ( $\text{EW}(\text{H}\beta) \geq 50 \text{ \AA}$ ), and black open circles ( $\text{EW}(\text{H}\beta) < 50 \text{ \AA}$ ), respectively. On top are histograms of  $m(\text{FUV})_{\text{mod}} - m(\text{FUV})_{\text{obs}}$  distributions for the entire samples with  $\text{EW}(\text{H}\beta) \geq 50 \text{ \AA}$  and  $< 50 \text{ \AA}$  (black and grey lines, respectively). Vertical lines in all panels indicate equal values of  $m(\text{FUV})_{\text{obs}}$  and  $m(\text{FUV})_{\text{mod}}$  and horizontal bars are  $1\sigma$  dispersions of  $m(\text{FUV})_{\text{mod}} - m(\text{FUV})_{\text{obs}}$ .

blue continua. The He II emission line in spectra of selected CSFGs is very weak or absent, indicating that hard nonthermal ionising radiation is weak or absent in these galaxies. We use this sample in the present study.

The SDSS photometric and spectroscopic data were supplemented by *GALEX* photometric data in the UV range, *Wide-field Infrared Survey Explorer* (*WISE*), *Infrared Astronomical Satellite* (*IRAS*) and *Herschel* photometric data in the IR range to derive SEDs, stellar masses, luminosities and to compare observed and modelled apparent magnitudes in the far-UV (FUV) and near-UV (NUV) ranges.

Monte Carlo calculations were used to derive intrinsic

SEDs in the optical range. The method was described e.g. by [Izotov et al. \(2011, 2015\)](#). SF history in CSFGs was approximated by a recent instantaneous burst and by continuous SF with a constant SFR for old stellar populations. Both stellar and nebular continua and line emission were taken into account in the SED modelling. For fitting of the SEDs we use SDSS spectra corrected for extinction with the reddening law by [Cardelli et al. \(1989\)](#) with  $R(V) = 3.1$ . Varying  $R(V)$  in the range 2.7 – 4.5 results in differences less than a few percent between the SDSS spectra for our relatively transparent CSFGs ([Izotov et al. 2016c](#)). For stellar SEDs we adopted a Salpeter IMF ([Salpeter 1955](#)), Padova evolutionary tracks ([Girardi et al. 2000](#)) and a combination of stel-

lar atmosphere models by [Lejeune, Buser & Cuisiner \(1997\)](#) and [Schmutz, Leitherer & Gruenwald \(1992\)](#). The output quantities of the Monte Carlo modelling are ages and masses of the young burst and the old stellar population with which SDSS spectra are best reproduced.

Aperture- and extinction-correction, and transformation of fluxes to the luminosities were described in [Izotov et al. \(2015\)](#).

The general properties of our SDSS DR12 sample of CSFGs are discussed by [Izotov et al. \(2016c\)](#). In many respects they are similar to the properties of high- $z$  SFGs. In addition, we show in Fig. 1 the distribution of the  $[\text{O III}]\lambda 5007\text{\AA}/\text{H}\beta$  emission-line ratio on the galaxy stellar mass. Spectra of most CSFGs have high line ratios indicating active ongoing SF and young starburst ages.

Our galaxies are well overlapping with  $z \sim 3.5$  Lyman-break galaxies (LBGs) ([Schenker et al. 2013](#); [Troncoso et al. 2014](#); [Holden et al. 2016](#)) implying similar physical conditions in their ISMs. However, because of proximity the distribution of CSFGs extends to lower luminosities and stellar masses by almost three orders of magnitude. There is a slight increase of the  $[\text{O III}]/\text{H}\beta$  and then its slight decrease with the stellar mass for galaxies with high  $\text{EW}(\text{H}\beta)$ . This behaviour is predicted by photoionisation H II region models and is explained by higher metallicity and hence by the lower electron temperature in H II regions of more massive galaxies. The decrease of  $[\text{O III}]/\text{H}\beta$  at high stellar masses is more prominent for galaxies with low  $\text{EW}(\text{H}\beta)$ . It is caused not only by the lower electron temperature in H II regions of more massive galaxies, but also by considerable softening of ionising radiation at higher metallicities in bursts with high age (or low  $\text{EW}(\text{H}\beta)$ ), which is insufficient to produce ion  $\text{O}^{2+}$  in large quantities.

### 3 REDDENING IN THE UV RANGE

#### 3.1 Modelled apparent magnitudes in the UV range

We use extrapolations of SEDs derived from the optical SDSS spectra to obtain apparent FUV magnitudes<sup>1</sup>:

$$m(\text{FUV})_{\text{mod}} = -2.5 \log \int \frac{I(\lambda)Q_{\text{FUV}}(\lambda)d\lambda}{10^{[1+f(\lambda_0)]C(\text{H}\beta)}} - 18.31, \quad (1)$$

where  $I(\lambda)$  is the flux of the intrinsic SED at the observed wavelength  $\lambda$  attenuated by the (small) Milky Way extinction adopting a [Cardelli et al. \(1989\)](#) reddening law with  $R(V) = 3.1$  and expressed in  $\text{erg s}^{-1} \text{cm}^{-2} \text{\AA}^{-1}$ ,  $C(\text{H}\beta)$  is the galaxy's intrinsic extinction coefficient derived from the hydrogen Balmer decrement after correction for the Milky Way extinction, which depends on  $A(V)$  and  $R(V)$  (see Eq. 1 in [Izotov et al. 2016a](#)),  $\lambda_0 = \lambda/(1+z)$  is the rest-frame wavelength,  $f(\lambda_0) = 0.4 \times [A(\lambda_0)/C(\text{H}\beta) - 1]$ , and  $Q_{\text{FUV}}(\lambda)$  is the transmission of the GALEX FUV filter.<sup>2</sup>

<sup>1</sup> [http://asd.gsfc.nasa.gov/archive/galex/FAQ/counts\\_back\\_ground.html](http://asd.gsfc.nasa.gov/archive/galex/FAQ/counts_back_ground.html)

<sup>2</sup> <http://svo2.cab.inta-csic.es/svo/theory/fps3/index.php?id=GALEX/GALEX.FUV&&mode=browse&gname=GALEX&gname2=GALEX#filter>

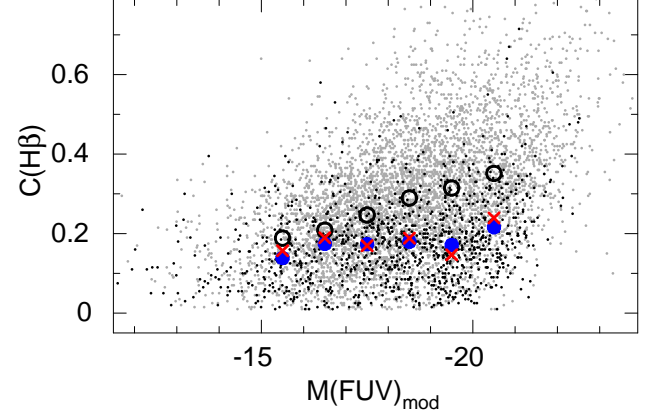


**Figure 3.** The dependence of the extinction coefficient  $C(\text{H}\beta)$  on the modelled rest-frame absolute FUV magnitude  $M(\text{FUV})_{\text{mod}}$ . Symbols are same as in Fig. 2.

Similarly, the apparent NUV magnitudes are derived as

$$m(\text{NUV})_{\text{mod}} = -2.5 \log \int \frac{I(\lambda)Q_{\text{NUV}}(\lambda)d\lambda}{10^{[1+f(\lambda_0)]C(\text{H}\beta)}} - 19.17, \quad (2)$$

where  $Q_{\text{NUV}}(\lambda)$  is the transmission of the GALEX NUV filter.<sup>3</sup>

The rest-frame extinction-corrected absolute magnitudes are obtained as

$$M(\text{FUV})_{\text{mod}} = -2.5 \log \int I_0(\lambda_0)Q_{\text{FUV}}(\lambda_0)d\lambda_0 - 43.31 + 5 \log D \quad (3)$$

and

$$M(\text{NUV})_{\text{mod}} = -2.5 \log \int I_0(\lambda_0)Q_{\text{NUV}}(\lambda_0)d\lambda_0 - 44.17 + 5 \log D, \quad (4)$$

where  $I_0(\lambda_0)$  is the flux of the intrinsic SED at the rest-frame wavelength  $\lambda_0$ ,  $D$  is the luminosity distance derived with a cosmological calculator (NASA Extragalactic Database (NED), [Wright 2006](#)), based on the cosmological parameters  $H_0=67.1 \text{ km s}^{-1} \text{Mpc}^{-1}$ ,  $\Omega_\Lambda=0.682$ ,  $\Omega_m=0.318$  ([Planck Collaboration XVI 2014](#)).

#### 3.2 Comparison of modelled and observed apparent FUV and NUV magnitudes

The aim of this Section is to study how well modelled FUV and NUV apparent magnitudes reproduce the observed data. We also wish to put constraints on the reddening law in the UV range.

In Fig. 2 we show dependencies of the differences between modelled and observed apparent FUV magnitudes on the absolute FUV magnitudes for  $\sim 7400$  CSFGs detected by GALEX in the FUV range, where modelled magnitudes  $m(\text{FUV})_{\text{mod}}$  are derived from the intrinsic SEDs, which are attenuated adopting extinction coefficients  $C(\text{H}\beta)$  and the [Cardelli et al. \(1989\)](#) reddening law with various  $R(V)$ s (Figs. 2a-c) and the [Calzetti et al. \(1994\)](#) reddening

<sup>3</sup> <http://svo2.cab.inta-csic.es/svo/theory/fps3/index.php?id=GALEX/GALEX.NUV&&mode=browse&gname=GALEX&gname2=GALEX#filter>

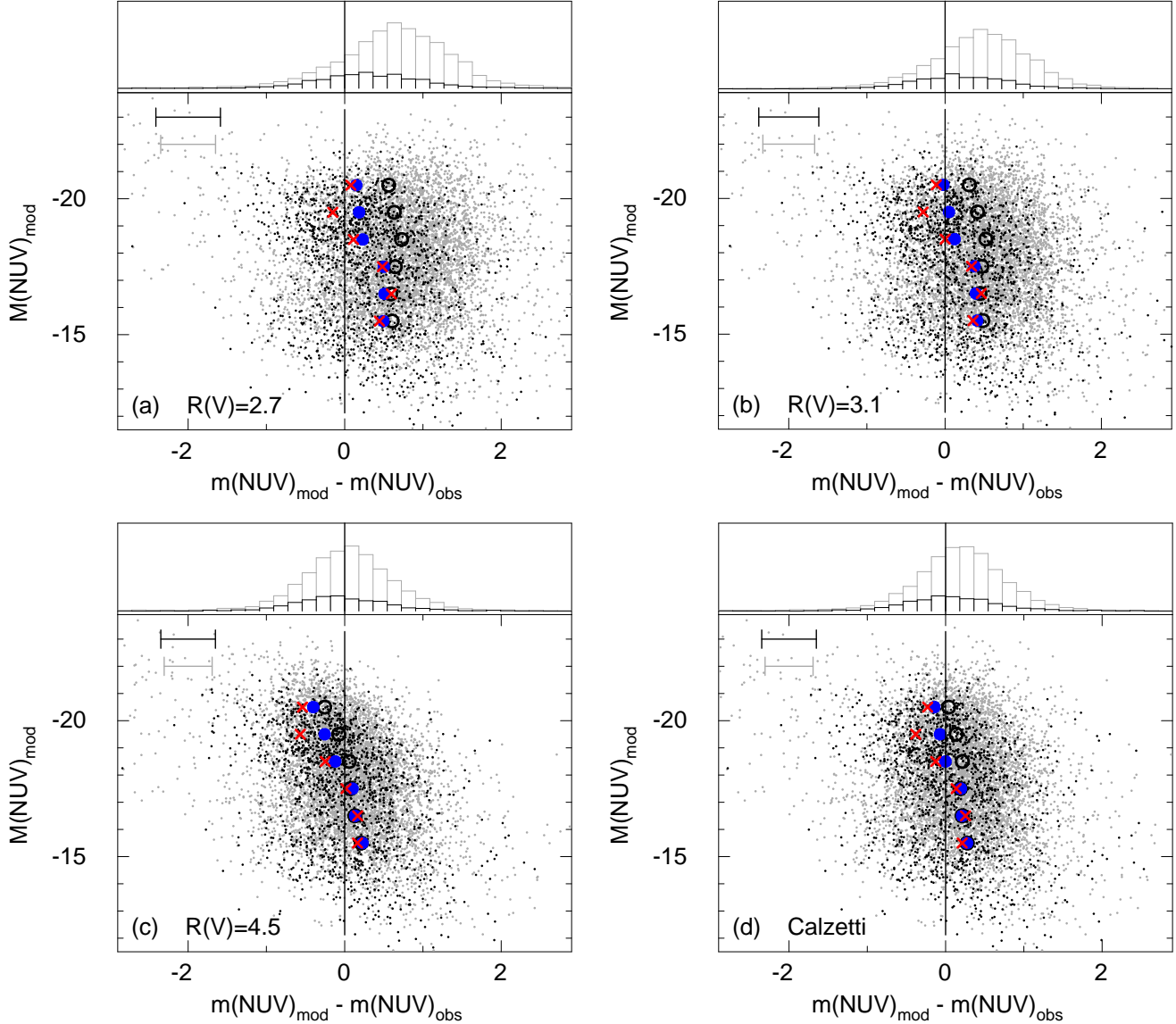


Figure 4. Same as in Fig. 2 but for NUV magnitudes.

law (Fig. 2d) (hereafter obscured SEDs). In all panels, the sample is split into galaxies with  $\text{EW}(\text{H}\beta) \geq 50\text{\AA}$  (black dots) and with  $\text{EW}(\text{H}\beta) < 50\text{\AA}$  (grey dots). The respective average values of  $m(\text{FUV})_{\text{mod}} - m(\text{FUV})_{\text{obs}}$  in 1 mag bins of  $M(\text{FUV})_{\text{mod}}$  are shown by blue filled and black open circles. Additionally, by red crosses we show average values for the youngest starbursts with  $\text{EW}(\text{H}\beta) \geq 150\text{\AA}$ . Equal modelled and observed apparent magnitudes are indicated by vertical lines. On top of each panel are histograms of the  $m(\text{FUV})_{\text{mod}} - m(\text{FUV})_{\text{obs}}$  distribution for CSFGs with  $\text{EW}(\text{H}\beta) \geq 50\text{\AA}$  (black line) and  $\text{EW}(\text{H}\beta) < 50\text{\AA}$  (grey line).

It is seen in Fig. 2 that  $m(\text{FUV})_{\text{mod}}$  most strongly depends on  $R(V)$  for intrinsically brighter galaxies with  $\text{EW}(\text{H}\beta) < 50\text{\AA}$ . This appearance can be explained by the fact that the average extinction in these galaxies is higher than in fainter galaxies with  $\text{EW}(\text{H}\beta) < 50\text{\AA}$  (black open circles in Fig. 3). This is consistent with conclusions made by e.g. Pannella et al. (2015) for GOODS-N galaxies at  $z \sim 2$ . We also note that average extinction in our CSFGs with

higher  $\text{EW}(\text{H}\beta)$  (blue filled circles and red crosses in Fig. 3) is lower and weakly depends on the galaxy intrinsic brightness.

The agreement between the observed and modelled magnitudes for galaxies with high  $\text{EW}(\text{H}\beta) \geq 50\text{\AA}$  (blue filled circles) is essentially the same for reddening laws with  $R(V) = 2.7$  and 3.1 excluding CSFGs with  $M(\text{FUV})_{\text{mod}}$  fainter than  $-16$  mag (Figs. 2a,b). However, since average  $m(\text{FUV})_{\text{mod}} - m(\text{FUV})_{\text{obs}}$  values for  $R(V) = 2.7$  and 3.1 are located to the right and to the left from the line of equal magnitudes, respectively, the most appropriate value for  $R(V)$  would be between 2.7 and 3.1. Considering only galaxies with youngest starbursts as determined by their high  $\text{EW}(\text{H}\beta) \geq 150\text{\AA}$  we conclude that a reddening law with  $R(V) = 2.7$  is more preferable. This is supported by SED fitting of the *HST*/COS spectra in combination with SDSS spectra of five LyC escaping galaxies with high  $\text{EW}(\text{H}\beta) \sim 200\text{\AA}$ . Izotov et al. (2016a,b) showed that the observed data are best fitted with the obscured SEDs adopting an extinc-

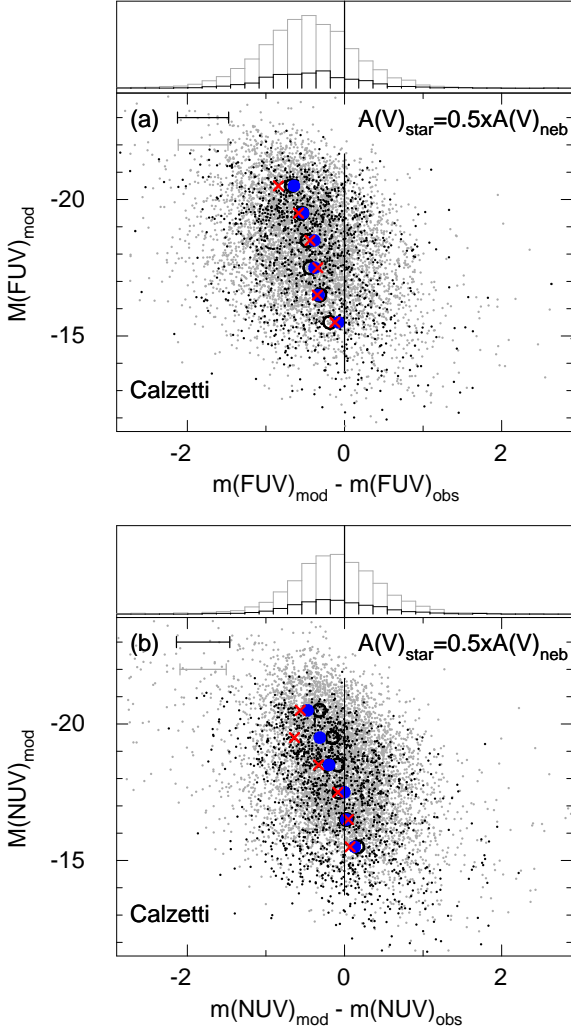


**Figure 5.** (a) The dependence of the difference between modelled and observed apparent FUV magnitudes  $m(\text{FUV})_{\text{mod}} - m(\text{FUV})_{\text{obs}}$  on the modelled rest-frame absolute FUV magnitude  $M(\text{FUV})_{\text{mod}}$  adopting the Calzetti et al. (1994) reddening law and stellar extinction equal to half of the nebular extinction. (b) The same for the modelled rest-frame absolute NUV magnitude  $M(\text{NUV})_{\text{mod}}$ . For the symbols, see Fig. 2.

tion law somewhat steeper in the FUV range than the widely used law with  $R(V) = 3.1$ . On the other hand, the agreement is worse if the Calzetti et al. (1994) reddening law is adopted (Fig. 2d) with further worsening for a shallower reddening law with  $R(V) = 4.5$  (Fig. 2c).

The agreement for galaxies with low  $\text{EW}(\text{H}\beta) < 50\text{\AA}$  (black open circles) is the best if the Cardelli et al. (1989) reddening law with  $R(V) = 3.1$  or the Calzetti et al. (1994) reddening law are adopted (Figs. 2b,d).

Steepening of the reddening curve, corresponding to lower  $R(V)$ , with increasing  $\text{EW}(\text{H}\beta)$  may imply that intense UV radiation, which is higher in galaxies with high  $\text{EW}(\text{H}\beta)$ s, modifies the size distribution of dust grains indicating a larger fraction of small dust grains. Higher  $\text{EW}(\text{H}\beta)$ s imply younger ages of starbursts and correlate with higher ionisation parameters and thus with higher  $[\text{O III}]/[\text{O II}]$  emission-line flux ratios. The modelled apparent

FUV magnitudes of galaxies with high  $[\text{O III}]/[\text{O II}]$  better reproduce observed magnitudes if low  $R(V)$ s are adopted. This is consistent with the conclusions made for low-redshift Lyman continuum leaking galaxies (Izotov et al. 2016a,b).

Somewhat different conclusions can be drawn from dependencies of differences between modelled and observed NUV magnitudes on absolute NUV magnitudes for  $\sim 7900$  CSFGs detected by GALEX in the NUV range (Fig. 4). At variance with the FUV wavelength range, the reddening curve in the NUV range in the case of Cardelli et al. (1989) approximations is non-monotonic and includes the bump at  $2175\text{\AA}$ . It is seen that a better agreement between models and observations for the CSFGs can be achieved with the Calzetti et al. (1994) reddening law or with the Cardelli et al. (1989) reddening law with  $R(V) = 4.5$ , excluding bright young starbursts shown by red crosses, where  $R(V) = 2.7$  is more appropriate, similar to the FUV range. Fig. 4 demonstrates that in general the reddening law by Cardelli et al. (1989) with a fixed  $R(V)$  may not reproduce at the same time FUV and NUV magnitudes of CSFGs, requiring systematically lower  $R(V)$  at shorter wavelengths. Therefore, the reddening law in CSFGs may deviate from that of Cardelli et al. (1989).

It was shown by Calzetti et al. (1994) that empirical curves for SFGs completely lack the  $2175\text{\AA}$  feature. Later, Czerny et al. (2004) and Gaskell et al. (2004) also found that empirical reddening curves for AGNs lack this feature. Therefore, we examine this possibility for our CSFGs, removing this feature from Cardelli et al. (1989) reddening curves and replacing it by a simple linear interpolation between wavelengths  $1800\text{\AA}$  and  $2500\text{\AA}$ . This modification would result in lower extinction in the NIR range and thus brighter  $m(\text{NUV})_{\text{mod}}$ . However, on average, the effect for our CSFGs is very small, not exceeding  $0.1$  mag compared to the case with the  $2175\text{\AA}$  feature.

The even distribution of the differences between the modelled and observed apparent magnitudes around zero value in Figs. 2 and 4 with dispersion of  $\sim 0.7$  mag suggests that the main source of the data spread are the extinction uncertainties of  $\sim 1$  mag in the FUV and NUV ranges, which translate to uncertainties of  $\leq 0.1 - 0.2$  mag in the V-band extinction  $A(V)$  and correspondingly  $\leq 0.1$  in  $C(\text{H}\beta)$ . This is the typical uncertainty of the extinction coefficient determination from the hydrogen Balmer decrement. Furthermore, the errors of GALEX magnitudes for our faint CSFGs are relatively high and can reach up to  $\sim 0.3 - 0.5$  mags. This further increases the dispersion in Fig. 4.

In the above discussion we assumed that the extinction for nebular and stellar radiation are equal. This assumption may not be valid. In particular, it was argued by e.g. Calzetti et al. (2000) that the ratio of the stellar extinction to the nebular extinction for local SFGs is only  $0.44$  and may vary in the range  $0.44 - 1.0$  for both the local and high- $z$  SFGs (Calzetti 1997; Erb et al. 2006; Reddy et al. 2010; Kashino et al. 2013; Price et al. 2014; Pannella et al. 2015; Valentino et al. 2015; Puglisi et al. 2016). Low values of the ratio imply that stars and ionised gas are not co-spatial. In particular, this appearance is expected for the stars located in the holes which are surrounded by denser ionised gas clouds. High ratios are in favour of more uniform gas distributions around the stars.

We address this issue for our galaxies assuming that

the nebular extinction derived from the Balmer decrement is two times higher than the stellar extinction, but reddening laws are the same. Results are presented in Fig. 5a for the FUV range and in Fig. 5b for the NUV range assuming the Calzetti et al. (1994) reddening law. The effect is higher for the FUV magnitudes because of the higher extinction, but in both diagrams modelled brightnesses are overpredicted with a clear trend toward higher intrinsic galaxy luminosities, while differences in  $m(\text{FUV})_{\text{mod}} - m(\text{FUV})_{\text{obs}}$  and  $m(\text{NUV})_{\text{mod}} - m(\text{NUV})_{\text{obs}}$  are much lower for the case with equal nebular and stellar extinctions (Figs. 2d and 4d). The conclusions are not changed if dependencies of  $m(\text{FUV})_{\text{mod}} - m(\text{FUV})_{\text{obs}}$  and  $m(\text{NUV})_{\text{mod}} - m(\text{NUV})_{\text{obs}}$  on SFR or  $M_{\star}$  are considered, because these integrated characteristics correlate with  $M(\text{FUV})$  and  $M(\text{NUV})$ . This comparison favours small differences between the nebular and stellar extinctions.

#### 4 THE SLOPE OF THE UV CONTINUUM IN CSFGS

The shape of the UV continuum is widely used to study extinction in low- $z$  and high- $z$  SFGs. In particular, the empirical Calzetti et al. (1994) reddening law is parameterized by the slope  $\beta$  of the UV continuum adopting a power law flux distribution  $I(\lambda) \sim \lambda^{\beta}$ . We define the slopes  $\beta_{\text{int}}$  and  $\beta_{0,\text{int}}$  of the intrinsic and obscured SEDs, respectively:

$$\beta_{\text{int}} = \frac{\log I(\lambda_1) - \log I(\lambda_2)}{\log \lambda_1 - \log \lambda_2}, \quad (5)$$

$$\beta = \beta_{\text{int}} - 0.4 \times \frac{A(\lambda_1) - A(\lambda_2)}{\log \lambda_1 - \log \lambda_2}, \quad (6)$$

where  $\lambda_1=1300\text{\AA}$  and  $\lambda_2=1800\text{\AA}$  are rest-frame wavelengths,  $I_{\lambda}$  is intrinsic flux, which includes both the stellar and nebular emission, and  $A(\lambda)$  is the extinction in mags.

In Fig. 6a we show the dependence of the intrinsic slope  $\beta_{\text{int}}$  on the stellar masses  $M_{\star}$  of the  $\sim 14000$  galaxies from our sample. As in Figs. 2 – 5, the sample is split into CSFGs with low EW( $\text{H}\beta$ ) (grey dots) and high EW( $\text{H}\beta$ ) (black dots). We note that for galaxies whose optical light is dominated by young stars, as the case for most sources considered here, EW( $\text{H}\beta$ ) is primarily an age indicator. For other galaxies EW( $\text{H}\beta$ ) will be more sensitive to other parameters as the specific SFR.

A clear separation between these two CSFG subsamples is present with steeper slopes of  $\sim -2.3$  to  $-2.7$  for galaxies with high EW( $\text{H}\beta$ ), while slopes of the UV continuum in galaxies with EW( $\text{H}\beta$ )  $< 50\text{\AA}$  are  $\sim -1.8$  to  $-2.5$ . This is expected because star-forming regions in CSFGs with high EW( $\text{H}\beta$ ) from our sample have younger ages and the radiation of short bursts of SF is dominant in the UV range (Izotov et al. 2016c).

Adopting the starbursting scenario we apply the correction of the UV slope to reduce it to zero burst age assuming that SF occurs in a single instantaneous burst and using Starburst99 models (Leitherer et al. 1999, 2014). This correction includes both the stellar and nebular emission which both depend on the galaxy metallicity and the starburst age. Stellar emission is reduced to zero age adopting the dependencies of intrinsic fluxes at  $\lambda_1=1300\text{\AA}$  and  $\lambda_2=1800\text{\AA}$  on EW( $\text{H}\beta$ ) in Starburst99 instantaneous burst

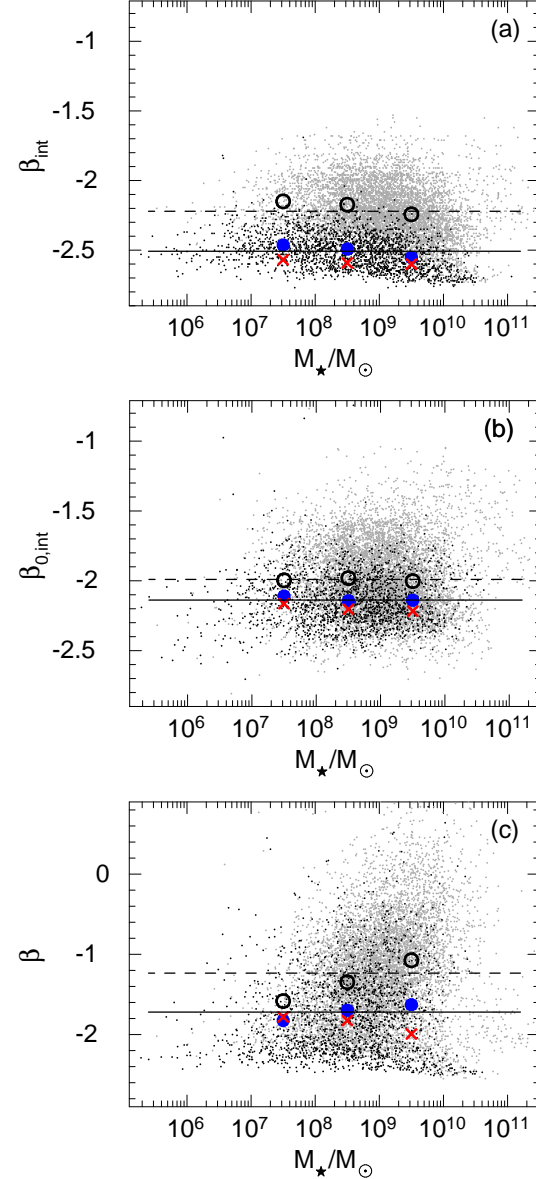


**Figure 6.** The dependence of (a) the intrinsic UV continuum slope  $\beta_{\text{int}}$  and (b) the intrinsic UV continuum slope  $\beta_{0,\text{int}}$ , reduced to zero starburst age, on the stellar mass of the galaxies. (c) Same as in (a) and (b), but UV continuum slopes  $\beta$  are derived from obscured SEDs with extinction coefficient  $C(\text{H}\beta)$  and adopting  $R(V) = 2.7$  for galaxies with  $\text{EW}(\text{H}\beta) \geq 50\text{\AA}$  (black dots) and  $R(V) = 3.1$  for galaxies with  $\text{EW}(\text{H}\beta) < 50\text{\AA}$  (grey dots). Solid and dashed horizontal lines in all panels are average values of  $\beta$  in CSFGs with high and low EW( $\text{H}\beta$ ), respectively. The average values in 1 dex bins of  $\log M_{\star}$  for CSFGs with  $\text{EW}(\text{H}\beta) \geq 150\text{\AA}$ ,  $\geq 50\text{\AA}$ , and  $< 50\text{\AA}$  are shown by red crosses, blue filled circles and black open circles, respectively.

models which depend also on the metallicity. As for nebular continuum at the same wavelengths, it was scaled up by the factor of  $\text{EW}(\text{H}\beta)_{t=0}/\text{EW}(\text{H}\beta)_{\text{obs}}$ , where  $\text{EW}(\text{H}\beta)_{\text{obs}}$  and  $\text{EW}(\text{H}\beta)_{t=0}$  are H $\beta$  equivalent widths observed and at the burst age  $t = 0$ , respectively. Finally, age-corrected slopes are derived from the sums of stellar and nebular emission at  $\lambda_1=1300\text{\AA}$  and  $\lambda_2=1800\text{\AA}$  using Eq. 5.

We present in Fig. 6b the dependence of the intrinsic

UV slope  $\beta_{0,\text{int}}$  reduced to a zero age on the galaxy stellar mass. Comparing with Fig. 6a we conclude that the age correction makes the slope flatter with average values shown by solid and dashed lines. The flattening is caused by the fact that the slope of the intrinsic stellar emission of the young starburst corresponding to  $\beta \sim -2.8$  is much steeper than the nebular emission with a slope corresponding to  $\beta \sim 0.0$ . The fraction of nebular emission for younger ages is higher making the slope of total stellar and nebular emission flatter. The correction for the burst age considerably reduces the offset between CSFGs with high and low  $\text{EW}(\text{H}\beta)$ s indicated by the difference of average  $\beta_{0,\text{int}}$  values (solid and dashed lines) confirming conclusions made earlier, e.g., by Izotov et al. (2011, 2015, 2016c) that SF in these galaxies mainly has a bursting nature.

Fig. 6c shows the dependence of the UV slopes  $\beta$  on stellar masses  $M_*$ .  $\beta$  has been derived from the obscured SEDs adopting extinction obtained from the Balmer decrement and reddening laws with  $R(V) = 2.7$  for galaxies with  $\text{EW}(\text{H}\beta) \geq 50\text{\AA}$  and with  $R(V) = 3.1$  for galaxies with  $\text{EW}(\text{H}\beta) < 50\text{\AA}$ . Stellar and interstellar extinction were assumed to be the same. The spread of slopes in this panel is much higher than in Figs. 6a,b implying that it is mainly determined by extinction, which is responsible for  $> 70\%$  of the spread, rather than by different starburst ages. The range of slopes  $\beta$  for our CSFGs is  $-2.5 - 0.6$ , similar to that for high-redshift UV-selected SFGs with  $z = 2 - 10$  (Finkelstein et al. 2012; Bouwens et al. 2014, 2016b). Average values of  $\beta$  shown in Fig. 6c by horizontal lines and various symbols are comparable to those for  $z \sim 4$  galaxies (Finkelstein et al. 2012) and for  $z > 1$  galaxies (Reddy et al. 2010, 2015; Kurczynski et al. 2014; Forrest et al. 2016; Matthee et al. 2016).

## 5 EFFICIENCY OF IONISING PHOTON PRODUCTION

We noted above that CSFGs are characterized by active star formation and have properties, which in many respects are similar to high- $z$  SFGs (Izotov et al. 2015). Because our galaxies produce a copious amount of ionising photons they can be considered as analogs of high- $z$  galaxies responsible for the reionisation of the Universe at redshifts  $z = 5 - 10$ . One of the important parameters regulating the intergalactic medium (IGM) ionisation is the LyC escape fraction  $f_{\text{esc}}(\text{LyC})$ . Izotov et al. (2016a,b) have shown that the absolute escape fraction  $f_{\text{esc}}(\text{LyC})$  in local CSFGs can be as high as  $\sim 10\%$ . Another parameter is the efficiency of ionising photon production determined as

$$\xi = \frac{N(\text{LyC})}{L_\nu}, \quad (7)$$

where  $N(\text{LyC})$  is the Lyman continuum photon production rate,  $L_\nu$  is the intrinsic monochromatic luminosity at the rest-frame wavelength of  $1500\text{\AA}$ .  $L_\nu$  in our galaxies is derived from the SED fitting, while the Lyman continuum photon production rate is derived from the relation using the extinction-corrected H $\beta$  luminosity  $L(\text{H}\beta)$  according to Storey & Hummer (1995):

$$N(\text{LyC}) = 2.1 \times 10^{12} L(\text{H}\beta), \quad (8)$$

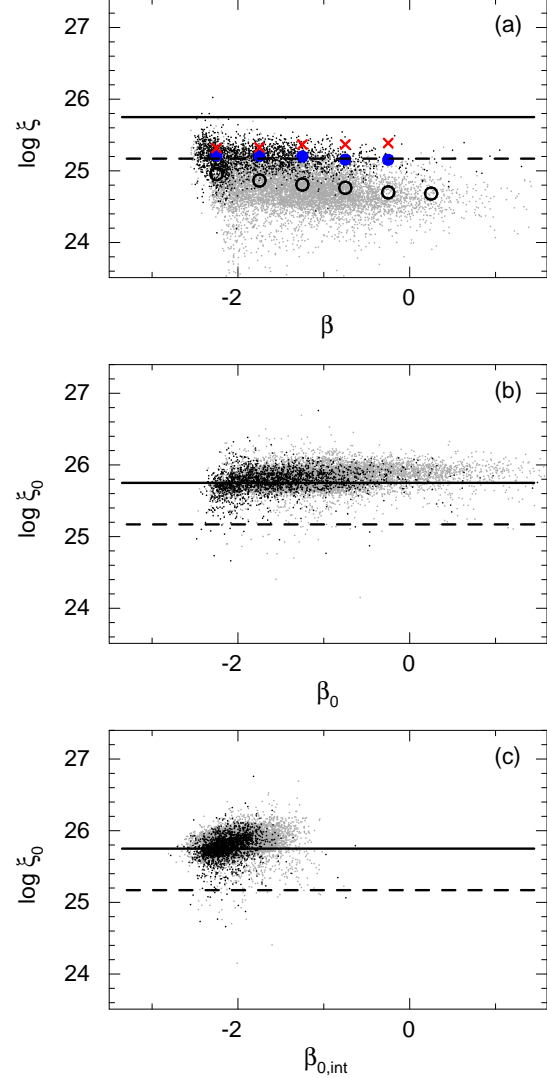


**Figure 7.** (a) The dependence of the efficiency of ionising photon production  $\xi$  on the UV continuum slope  $\beta$  of the obscured SEDs with the extinction derived from the hydrogen Balmer decrement in the SDSS spectra and adopting  $R(V) = 2.7$  for galaxies with  $\text{EW}(\text{H}\beta) \geq 50\text{\AA}$  (black dots) and  $R(V) = 3.1$  for galaxies with  $\text{EW}(\text{H}\beta) < 50\text{\AA}$  (grey dots), while blue filled and black open circles represent respective  $\log \bar{\xi}$  in 0.5 bins of  $\beta$ , where  $\bar{\xi}$  are average  $\xi$  values. Additionally,  $\log \bar{\xi}$  for CSFGs with  $\text{EW}(\text{H}\beta) \geq 150\text{\AA}$  are shown by red crosses. (b) same as in (a) but  $\xi_0$  (the efficiency of ionising photon production) and  $\beta_0$  (the obscured continuum UV slope) are both reduced to zero age. (c) same as in (b) but  $\beta_{0,\text{int}}$  is the slope of the intrinsic UV continuum. Solid and dashed horizontal lines in all panels indicate ionising photon production for zero-age instantaneous bursts and for continuous SF, respectively.

where  $N(\text{LyC})$  and  $L(\text{H}\beta)$  are in units  $\text{s}^{-1}$  and  $\text{erg s}^{-1}$ , respectively. Knowing  $f_{\text{esc}}(\text{LyC})$  and  $\xi$  it is possible to compute the total photon rate at which a galaxy population ionises the IGM (e.g. Robertson et al. 2013). The production efficiency  $\xi$  of a given stellar population is a simple prediction from synthesis models, which depends on metallicity, star-formation history, age, and also on assumptions on stellar evolution. Typically canonical values of  $\log \xi \sim 25.2 - 25.3$  are adopted for high- $z$  studies, where  $\xi$  is expressed in



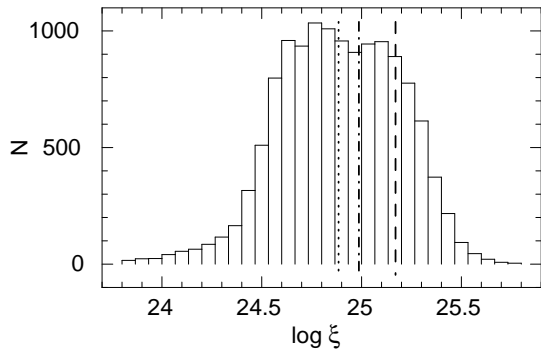


**Figure 8.** The histogram of the efficiency of ionising photon production  $\xi$  distribution for the entire CSFG sample. Dotted and dash-dotted vertical lines indicate  $\log \bar{\xi}$  and  $\log \bar{\xi}$ , which are the average value of  $\log \xi$  and the log of the average value of  $\xi$ , respectively. The value of  $\log \xi$  for the model with continuous star formation is shown by the dashed vertical line.

$\text{erg}^{-1}\text{Hz}$ . Observationally  $\xi$  has recently been estimated by Bouwens et al. (2015) for a sample of high- $z$  LBGs, finding values of  $\xi$  compatible with the canonical value. However, the ionising photon production of galaxies known to be LyC leakers (i.e. with  $f_{\text{esc}}(\text{LyC}) > 0$ ) has not been measured until recently. First determinations in five low- $z$  LyC leakers were presented by Schaerer et al. (2016) who found  $\log \xi \sim 25.1 - 25.5$ .

In this paper we derive the production efficiency for all  $\sim 14000$  CSFGs selected from the SDSS. Fig. 7a shows the dependence of  $\xi$  on the slope  $\beta$  of the obscured SED for CSFGs with  $\text{EW}(\text{H}\beta) \geq 50\text{\AA}$  (black dots) and  $\text{EW}(\text{H}\beta) < 50\text{\AA}$  (grey dots). It is seen that data scatter in a wide range  $\log \xi \sim 24.5 - 25.8$  with highest values for CSFGs with highest  $\text{EW}(\text{H}\beta)$ . Black open circles, blue filled circles and red crosses show logs of average values  $\bar{\xi}$  of  $\xi$  in 0.5 bins of  $\beta$  for CSFGs with  $\text{EW}(\text{H}\beta) < 50\text{\AA}$ ,  $\geq 50\text{\AA}$  and  $\geq 150\text{\AA}$ , respectively. The average values of  $\xi$  in log scale are  $\log \bar{\xi} \sim 24.82$ ,  $\sim 25.21$  and  $\sim 24.93$  for CSFGs with  $\text{EW}(\text{H}\beta) \geq 50\text{\AA}$ , with  $\text{EW}(\text{H}\beta) < 50\text{\AA}$ , and for the entire sample, respectively. Selecting only galaxies with  $[\text{O III}]/[\text{O II}] \gtrsim 5$  (the values characteristic of LyC escaping galaxies, Izotov et al. 2016a,b) we obtain  $\log \bar{\xi} = 25.31$ . All these values are similar to the canonical value implying that CSFGs could be important contributors of escaping ionising radiation capable to ionise the IGM. The dispersion of  $\xi$  is likely not dominated by uncertainties in the dust corrections. Although these uncertainties might be relatively high with dispersion of  $\sim 0.7$  mag in the FUV range or 0.3 dex in  $L(1500\text{\AA})$  (see Sect. 3), they can not produce an offset for CSFGs with high  $\text{EW}(\text{H}\beta)$  relative to the galaxies with low  $\text{EW}(\text{H}\beta)$ . IMF variations can be present but this is a highly speculative and uncertain topic, not warranted by observations.

A similar range of  $\log \xi$  is found for high- $z$  LBGs and Ly $\alpha$  emitters (LAEs) with  $z \sim 3 - 7.7$  (Bouwens et al. 2015; Nakajima et al. 2016; Stark et al. 2017). Comparing our values of  $\xi$  for galaxies with high  $\text{EW}(\text{H}\beta)$  with those for  $z \sim 4 - 5$  galaxies by Bouwens et al. (2016a) we find good agreement. The range of  $\log \xi$  for our galaxies (black dots) is also consistent with the results of modelling by Wilkins et al. (2016) for different stellar population synthesis models. However,  $\log \xi$  of our entire sample of CSFGs is

on average higher than the average value of 24.77 for  $z = 2.2$  H $\alpha$  emitting galaxies by Matthee et al. (2016).

The distribution of  $\xi$ s for CSFGs with the lowest  $\text{EW}(\text{H}\beta)$  (grey dots in Fig. 7a) shows a trend of decreasing  $\xi$  with increasing  $\beta$ . On the other hand, no such trend is detected for CSFGs with higher  $\text{EW}(\text{H}\beta)$ s.

For comparison, solid and dashed lines in Fig. 7a represent the values of  $\log \xi$  for the Starburst99 zero-age instantaneous burst models and the models with continuous SF with constant SFR, respectively. They take into account the contribution of both the stellar and nebular emission at  $1500\text{\AA}$  and are consistent with the respective values derived by Reiter, Schaerer & Fosbury (2010) for heavy element mass fraction greater than  $10^{-2}$ .

A histogram of the  $\xi$  distribution for the entire sample of CSFGs is shown in Fig. 8. The average value  $\bar{\xi}$  of  $\xi$  shown by dash-dotted line is  $\lesssim 1.5$  times lower than the value for the model with continuous SF (dashed line). However, the average values of  $\xi$  for CSFGs with  $\text{EW}(\text{H}\beta) \geq 50\text{\AA}$  (blue filled circles in Fig. 7a) are very similar to the value for the model with continuous SF.

It is clear from Fig. 7a that the model with continuous SF fails to reproduce observations both for CSFGs with high and low  $\text{EW}(\text{H}\beta)$ , which scatter in a wide range around the dashed line. This model predicts nearly constant  $\text{EW}(\text{H}\beta) \sim 40 - 50\text{\AA}$  and constant  $\xi$ , while the range of  $\text{EW}(\text{H}\beta)$  for galaxies from our sample is  $\sim 10 - 400\text{\AA}$  and  $\xi$  varies by one order of magnitude. On the other hand, the models with the instantaneous bursts may be successful in reproducing observations. In this case  $\xi$  should rapidly vary with age of the burst. The bursting nature of star formation is a reason why distributions of CSFGs with high and low  $\text{EW}(\text{H}\beta)$  are different in Fig. 7a. To show this we need to reduce the efficiency of ionising photon production to zero burst age, which we denote as  $\xi_0$ . For this we use Starburst99 models with appropriate metallicities (Leitherer et al. 1999, 2014) taking into account both the stellar and nebular emission in the continuum at  $1500\text{\AA}$ .

As it could be seen in Fig. 7b, distributions of  $\xi_0$  for CSFGs with high and low  $\text{EW}(\text{H}\beta)$ s are similar. There is a small upward offset of CSFGs with low  $\text{EW}(\text{H}\beta)$  (grey dots) relative to the value of the zero-age instantaneous burst model (solid line). This can be accounted for by the non-negligible contribution of an older stellar population to the continuum near the H $\beta$  emission line, which is higher for galaxies with lower  $\text{EW}(\text{H}\beta)$ . As a result, the age correction would be overestimated if the instantaneous burst model is taken. However, since the upward offset is only  $\leq 0.1$  dex, the assumption of an instantaneous burst model is reasonable. This assumption is further supported by Fig. 7c, where the distribution of  $\xi_0$  on the intrinsic UV slope reduced to zero age,  $\beta_{0,\text{int}}$ , is shown. Both  $\xi_0$  and  $\beta_{0,\text{int}}$  occupy a small region with dispersions, which can be caused by uncertainties of extinction determination, SED fitting and reduction to zero burst age, but in general the distribution of CSFGs is well reproduced by the instantaneous burst models.

We note, however, that the assumption of a continuous SF with constant SFR could be a reasonable approximation in estimating the average global efficiency of ionising photon production, e. g., in the early Universe during the epoch of reionisation if it is assumed that during that epoch first galaxies were formed with a constant rate, despite the

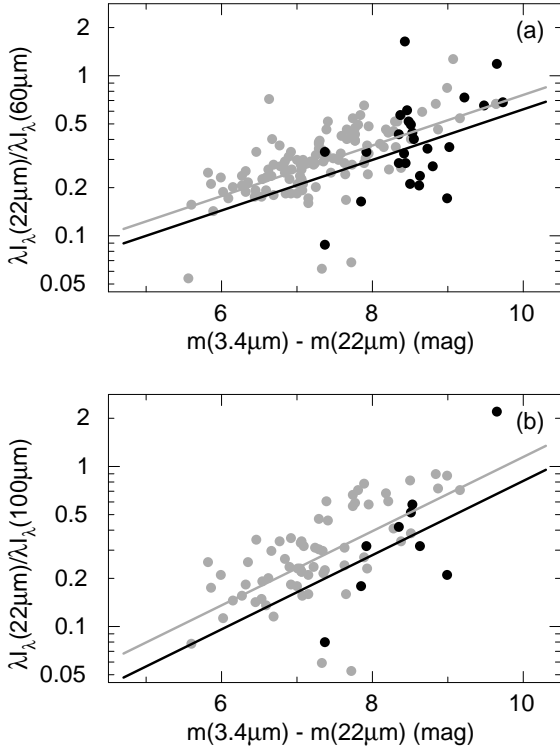


**Figure 9.** The relations between (a) the  $22\mu\text{m}/60\mu\text{m}$  intensity ratio and (b) the  $22\mu\text{m}/100\mu\text{m}$  intensity ratio on the *WISE*  $3.4\mu\text{m} - 22\mu\text{m}$  colour for the galaxies from our SDSS sample, which were detected by *IRAS* at  $60\mu\text{m}$  and  $100\mu\text{m}$ , respectively. The galaxies with  $\text{EW}(\text{H}\beta) \geq 50\text{\AA}$  and  $\text{EW}(\text{H}\beta) < 50\text{\AA}$  are shown by black and grey filled circles, respectively. Grey lines are maximum likelihood regressions for galaxies with  $\text{EW}(\text{H}\beta) < 50\text{\AA}$ , while black lines are relations adopted for galaxies with  $\text{EW}(\text{H}\beta) \geq 50\text{\AA}$ .

fact that SF in individual galaxies proceeded during short bursts. Thus, the value  $\log \xi = 25.17$  shown in Fig. 7 by the dashed line, similar to estimates in earlier studies (e.g. Robertson et al. 2013), is a reasonable estimate, which could be used in studies of the reionisation of the Universe. However, it may be somewhat higher in the early Universe because of lower stellar metallicities and a more top-heavy IMF of stars (e.g. Reiter et al. 2010).

## 6 THE RADIATION ENERGY BALANCE IN CSFGs

### 6.1 Luminosities in the UV range

To study the radiation energy balance of the CSFGs we derive the energy emitted by the galaxy in the UV and optical wavelength range at  $\lambda < 1\mu\text{m}$  using modelled SEDs:

$$L(\text{int}) = 4\pi D^2 \int_0^{1\mu\text{m}} I_\lambda d\lambda, \quad (9)$$

where  $I_\lambda$  is the intrinsic SED flux at the rest-frame wavelength  $\lambda$  and  $D$  is the distance.

Similarly, the absorbed luminosity is determined as

$$L(\text{abs}) = 4\pi D^2 \exp(\sqrt{1-\omega} - 1) \times \int_0^{1\mu\text{m}} I_\lambda [1 - 10^{-(1+f_\lambda)C(\text{H}\beta)}] d\lambda, \quad (10)$$

where term  $\exp(\sqrt{1-\omega} - 1)$  is the fraction of the absorbed radiation relative to the sum of absorbed and scattered radiation,  $\omega$  is the albedo of grains. Here we assume that scattering is isotropic (Calzetti et al. 1994) and  $\omega$  does not depend on the wavelength. The value of  $\omega$  in the UV is uncertain. Draine (2003) estimated  $\omega \sim 0.3 - 0.4$ , while Hurwitz, Bowyer & Martin (1991) found it to be  $< 0.25$  and scattering is fairly isotropic. For clarity, we adopt  $\omega = 0.3$ . The derived value of  $L(\text{abs})$  in the case of  $\omega = 0$  (no scattering) would be higher by  $\sim 13\%$ . We neglected a small contribution of the absorbed stellar and nebular radiation at  $\lambda > 1\mu\text{m}$  because of the very low extinction and low  $I_\lambda$  at these wavelengths.

### 6.2 Emission in the infrared range

For the determination of the luminosity in the infrared range we selected those CSFGs, which were detected by *WISE* in all four bands at  $3.4\mu\text{m}$ ,  $4.6\mu\text{m}$ ,  $12\mu\text{m}$  and  $22\mu\text{m}$ , totalling  $\sim 3000$  of our  $\sim 14000$  CSFGs. We use this sample to select those 145 galaxies, which were detected by *IRAS* at  $60\mu\text{m}$  and the 74 galaxies seen at  $100\mu\text{m}$ . These numbers are much smaller than the number of CSFGs detected in the mid-infrared range by *WISE* in all four bands. Therefore, some assumptions need to be made to derive the IR fluxes in the far-infrared range. For instance, Bouwens et al. (2016b) assumed a certain average dust temperature in SFGs. The weakness of this approach is that the dust mass should be defined as well. Additionally, it was shown e.g. by Hunt et al. (2014) and Izotov et al. (2014b) that the dust emission in SFGs can not be reproduced by a model with a single dust temperature.

We adopt another approach and search for a simple recipe to derive fluxes at  $\lambda > 22\mu\text{m}$  using *WISE* fluxes and apparent magnitudes. In Fig. 9 we show dependencies of  $22\mu\text{m}$ -to- $60\mu\text{m}$  and  $22\mu\text{m}$ -to- $100\mu\text{m}$  flux ratios on the *WISE*  $3.4\mu\text{m} - 22\mu\text{m}$  colour indices for SDSS CSFGs. These dependencies for galaxies with  $\text{EW}(\text{H}\beta) < 50\text{\AA}$  can be approximated by linear relations

$$\log \frac{\lambda I_\lambda(22\mu\text{m})}{\lambda I_\lambda(60\mu\text{m})} = 0.158[m(3.4\mu\text{m}) - m(22\mu\text{m})] - 1.700 \quad (11)$$

and

$$\log \frac{\lambda I_\lambda(22\mu\text{m})}{\lambda I_\lambda(100\mu\text{m})} = 0.232[m(3.4\mu\text{m}) - m(22\mu\text{m})] - 2.258, \quad (12)$$

which are shown in Fig. 9 by grey lines. There is a slight offset from these relations for galaxies with higher  $\text{EW}(\text{H}\beta) \geq 50\text{\AA}$ . However, the statistics of these galaxies is too low to produce reliable regressions. Therefore, we simply shift regressions shown by grey lines using average offsets by  $\sim 0.10$  in Fig. 9a and by  $\sim 0.15$  in Fig. 9b to produce relations for galaxies with high  $\text{EW}(\text{H}\beta) \geq 50\text{\AA}$  (black lines in Fig. 9). All these relations are used to derive fluxes at  $60\mu\text{m}$  and  $100\mu\text{m}$  for the entire sample of CSFGs detected by *WISE* at  $3.4\mu\text{m}$  and  $22\mu\text{m}$ .

For longer wavelengths we use data for CSFGs by Rémy-Ruyer et al. (2013) obtained with the *Herschel* telescope at  $100\mu\text{m}$ ,  $160\mu\text{m}$ ,  $250\mu\text{m}$ ,  $350\mu\text{m}$  and  $500\mu\text{m}$  and

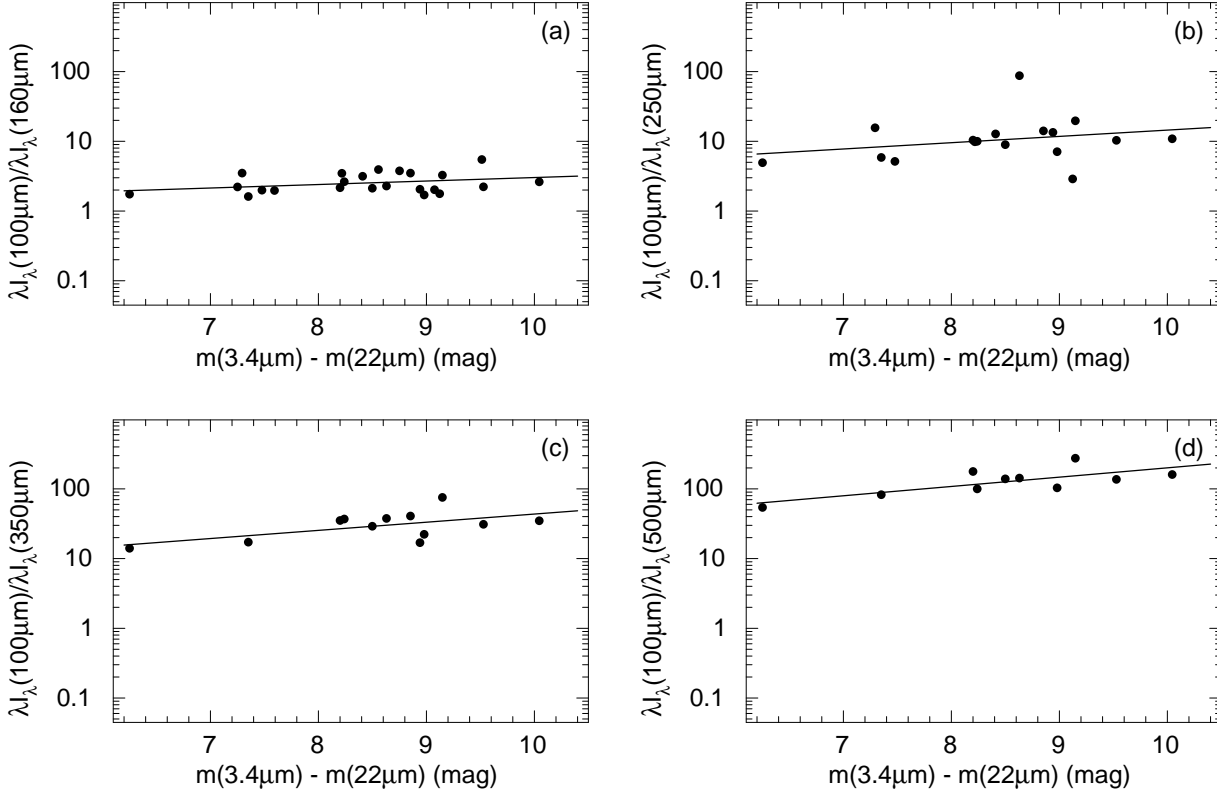


**Figure 10.** The relations between (a) the  $100\mu\text{m}/160\mu\text{m}$  intensity ratio, (b) the  $100\mu\text{m}/250\mu\text{m}$  intensity ratio, (c) the  $100\mu\text{m}/350\mu\text{m}$  intensity ratio and (d) the  $100\mu\text{m}/500\mu\text{m}$  intensity ratio on the *WISE*  $3.4\mu\text{m} - 22\mu\text{m}$  colour for the CSFGs by Rémy-Ruyer et al. (2013), which were detected by *Herschel* at  $100\mu\text{m}$ ,  $160\mu\text{m}$ ,  $250\mu\text{m}$ ,  $350\mu\text{m}$ , and  $500\mu\text{m}$ , respectively. Solid lines are maximum likelihood regressions.

derive the following relations (Fig. 10):

$$\log \frac{\lambda I_\lambda(100\mu\text{m})}{\lambda I_\lambda(160\mu\text{m})} = 0.050[m(3.4\mu\text{m}) - m(22\mu\text{m})] - 0.020, \quad (13)$$

$$\log \frac{\lambda I_\lambda(100\mu\text{m})}{\lambda I_\lambda(250\mu\text{m})} = 0.090[m(3.4\mu\text{m}) - m(22\mu\text{m})] + 0.258, \quad (14)$$

$$\log \frac{\lambda I_\lambda(100\mu\text{m})}{\lambda I_\lambda(350\mu\text{m})} = 0.117[m(3.4\mu\text{m}) - m(22\mu\text{m})] + 0.468, \quad (15)$$

$$\log \frac{\lambda I_\lambda(100\mu\text{m})}{\lambda I_\lambda(500\mu\text{m})} = 0.134[m(3.4\mu\text{m}) - m(22\mu\text{m})] + 0.964. \quad (16)$$

Finally, using mid-infrared fluxes obtained with *WISE* and the approximations presented in Eqs. 11 – 16 we derive luminosities emitted in the IR range at wavelengths  $8 - 1000 \mu\text{m}$ :

$$L(\text{IR}) = 4\pi D^2 \int_{8\mu\text{m}}^{1000\mu\text{m}} I_\lambda d\lambda. \quad (17)$$

### 6.3 Comparison of the absorbed UV radiation and IR emission

Using SEDs and Eq. 10 we derive the luminosity absorbed in the wavelength range  $\leq 1 \mu\text{m}$ . We restrict our sample and include only those CSFGs in which the extinction coefficient  $C(\text{H}\beta) > 0.1$  ( $\sim 4000$  galaxies), corresponding to an extinction  $A(V) \gtrsim 0.2$  mag. This is done because the uncertainties of the modelled absorbed luminosities are very high at low  $C(\text{H}\beta)$ s, which are comparable to their uncertainties. On the other hand, *WISE* fluxes and relations Eqs. 11 – 17 are used to derive the luminosity in the infrared range at  $\lambda = 8 - 1000 \mu\text{m}$ .

Independently derived luminosities  $L(\text{abs})$  and  $L(\text{IR})$  are compared in Fig. 11. It is seen in Fig. 11a that the luminosities absorbed at  $\lambda \leq 1\mu\text{m}$  are nearly equal to the luminosities emitted in the infrared range and do not depend on the galaxy stellar mass. There is also no dependence on the age of the starburst as indicated by the absence of an offset between CSFGs with high and low  $\text{EW}(\text{H}\beta)$ s (black and grey dots, respectively). The  $L(\text{IR})/L(\text{abs})$  ratio is increased by raising the slope of the obscured UV SED in Fig. 11b for  $\beta$  from  $\sim -1$  to  $-2$ , i.e. with decreasing extinction. The cause of the trend is not clear. On the other hand, this trend is absent at higher  $\beta$ . Perhaps, the trend appears because of the uncertainties in the determination of the infrared luminosities by using relations Eqs. 11 – 17. In any case, this trend is small and it does not change the general conclusion for the

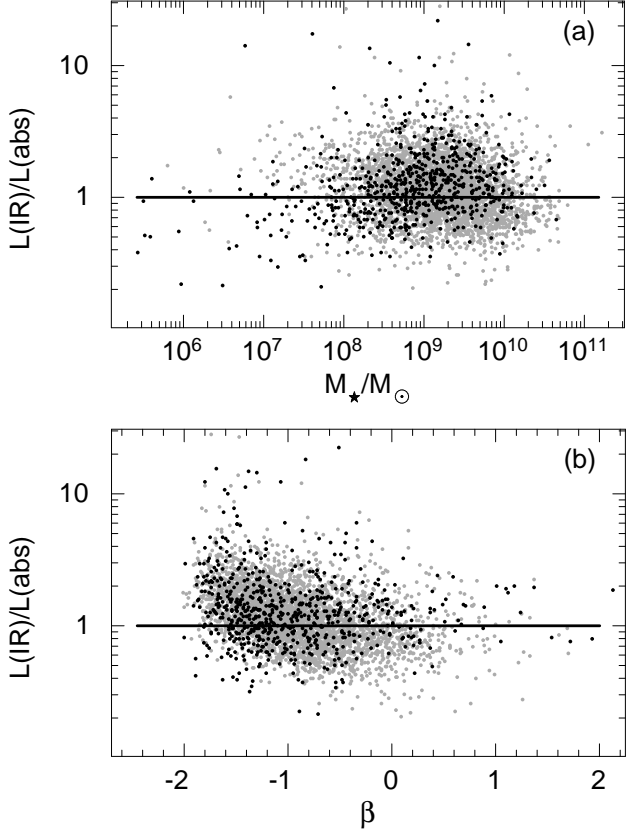


**Figure 11.** The dependencies of the ratios of the infrared luminosities  $L(\text{IR})$  in the wavelength range  $8 - 1000 \mu\text{m}$  and the luminosities  $L(\text{abs})$  absorbed in the wavelength range  $< 1 \mu\text{m}$  (a) on stellar masses and (b) on the obscured spectral UV slope adopting [Cardelli et al. \(1989\)](#) extinction laws with  $R(V) = 2.7$  for CSFGs with  $\text{EW}(\text{H}\beta) \geq 50 \text{\AA}$  (black dots) and  $3.1$  for CSFGs with  $\text{EW}(\text{H}\beta) < 50 \text{\AA}$  (grey dots) and extinction coefficients  $C(\text{H}\beta)$  which are derived from the hydrogen Balmer decrement in the SDSS spectra. Solid lines indicate equal  $L(\text{IR})$  and  $L(\text{abs})$ . The meaning of symbols is the same as in Fig. 2.

sample that on average the energy emitted in the IR range is equal to the energy of radiation absorbed in the star-forming regions, which are seen in the UV and optical ranges. Thus, there is no appreciable hidden SF which is not seen in the UV range. This result is in agreement with conclusions made by [Izotov & Thuan \(2011, 2016\)](#) and [Izotov et al. \(2009\)](#).

#### 6.4 Infrared excess

The infrared excess  $\text{IRX}$  is defined as the ratio of the observed luminosity of dust in the IR range to the observed UV luminosity. This quantity is somewhat arbitrary and depends on the adopted wavelength range in which the UV luminosity is derived. For the sake of comparison with other studies we define  $\text{IRX}$  as

$$\text{IRX} = \frac{L(\text{IR})}{\nu L_\nu}, \quad (18)$$

where  $\nu L_\nu$  are luminosities of the obscured SEDs at  $\lambda = 1500 \text{\AA}$ , which are proxies of observed luminosities.

The dependence of  $\text{IRX}$  on the UV slope of the

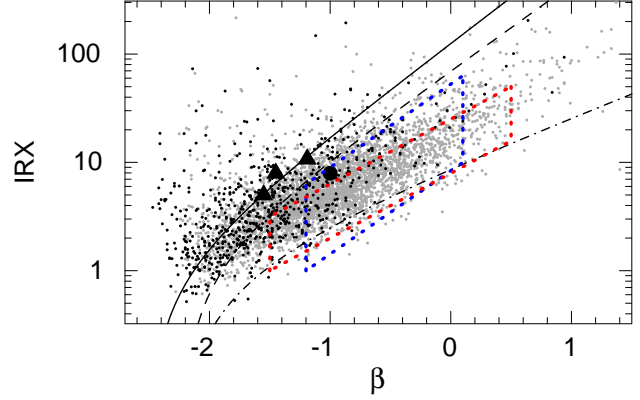


**Figure 12.** The dependencies of the SED infrared excesses  $\text{IRX}$  adopting [Cardelli et al. \(1989\)](#) reddening laws with  $R(V) = 2.7$  for CSFGs with  $\text{EW}(\text{H}\beta) \geq 50 \text{\AA}$  (black dots) and with  $R(V) = 3.1$  for CSFGs with  $\text{EW}(\text{H}\beta) < 50 \text{\AA}$  (grey dots) on the obscured spectral UV slopes  $\beta$ . Extinctions are derived from the hydrogen Balmer decrement in SDSS optical spectra. The average location of  $z \sim 2 - 3$  SFGs with stellar masses  $> 10^{9.75} M_\odot$  ([Bouwens et al. 2016b](#)) and different subsamples of SFGs at  $z \sim 2$  ([Reddy et al. 2012](#)) are shown by a filled circle and filled triangles, respectively. The distributions of SFGs by [Wang et al. \(2016\)](#) and [Boquien et al. \(2012\)](#) are indicated by regions delineated by blue and red dotted lines, respectively. For comparison, the dependencies for SFGs proposed by [Kong et al. \(2004\)](#) and [Meurer et al. \(1999\)](#) are shown by solid and dashed lines, while the dependence with the SMC reddening law by [Pettini et al. \(1998\)](#) is shown by a dash-dotted line.

observed SEDs is shown in Fig. 12. There are no offsets between the distributions of SFGs with high and low  $\text{EW}(\text{H}\beta)$ s. The distribution of our galaxies is overlapped with that of a sample of local galaxies from the Galaxy and Mass Assembly (GAMA) survey (region delineated by blue dotted lines, [Wang et al. 2016](#)) and SFGs from the Reference *Herschel* sample (region delineated by red dotted lines, [Boquien et al. 2012](#)), which however lack objects with steep slopes  $\beta \leq -1$  and  $\beta \leq -1.5$ , respectively. They also agree with the  $\text{IRX}$  values obtained by [Bouwens et al. \(2016b\)](#) and [Reddy et al. \(2012\)](#) for SFGs at  $z = 2 - 3$  (filled circle and filled triangles, respectively), and distributions of typical galaxies at  $z \sim 1 - 3$  ([Reddy et al. 2010](#); [Forrest et al. 2016](#)). The distribution of our CSFGs with  $\beta < -1.5$  is consistent with dependencies obtained by [Meurer et al. \(1999\)](#) (dashed line) and [Kong et al. \(2004\)](#) (solid line). On the other hand, the distribution of CSFGs with flatter slopes of beta is located between the dependencies obtained by [Meurer et al. \(1999\)](#) and [Kong et al. \(2004\)](#) on one side and the dependence by [Pettini et al. \(1998\)](#) (dash-dotted line) on the other side.

## 7 CONCLUSIONS

In this paper we model apparent and absolute far-UV (FUV) and near-UV (NUV) magnitudes of a sample of  $\sim 14000$  compact star-forming galaxies (CSFGs) selected from the Data Release 12 (DR12) of the Sloan Digital Sky Survey (SDSS). These quantities were obtained using extrapolations of spectral energy distributions (SEDs), which were obtained

from fitting the SDSS optical spectra. The modelled magnitudes are compared to observed *Galaxy Evolution Explorer* (GALEX) FUV and NUV magnitudes to constrain the reddening law in the UV range. We also derived the slopes of UV continua and efficiencies of ionised photon production using modelled SEDs and extinction-corrected  $H\beta$  luminosities. For the same CSFGs we derive intrinsic and absorbed luminosities in the UV range. These luminosities are compared to infrared (IR) luminosities, which were obtained using *Wide-field Infrared Survey Explorer* (WISE) fluxes at 3.4 - 22  $\mu\text{m}$  and various relations linking WISE fluxes with fluxes at longer wavelengths, 60 - 500  $\mu\text{m}$ , obtained with the *Infrared Astronomical Satellite* (IRAS) and *Herschel* observatories. Our main results are as follows.

1. We find that the differences between modelled and observed FUV and NUV apparent magnitudes depend on the adopted reddening law, which is used to obtain modelled apparent magnitudes from the CSFG' intrinsic SEDs in the UV range. The best agreement between the apparent and modelled FUV magnitudes for CSFGs with high equivalent widths of the  $H\beta$  emission line  $\text{EW}(H\beta) \geq 50\text{\AA}$  is found if the Cardelli et al. (1989) reddening law with  $R(V) = 2.7 - 3.1$  is adopted while  $R(V) = 2.7$  is found for CSFGs with  $\text{EW}(H\beta) \geq 150\text{\AA}$ . On the other hand, in CSFGs with  $\text{EW}(H\beta) < 50\text{\AA}$ , the best fit is achieved for observed apparent magnitudes adopting the Calzetti et al. (1994) reddening law or the Cardelli et al. (1989) reddening law with higher  $R(V) = 3.1$ . This implies that the properties of dust in SFGs with intense UV radiation, i.e. with high  $\text{EW}(H\beta)$ s, are characterized by a higher fraction of small grains resulting in a steeper reddening law. The agreement between the modelled and observed NUV magnitudes is better for slightly higher  $R(V)$  as compared to the FUV range indicating that one-parameter reddening laws by Cardelli et al. (1989) fail to reproduce observations in the entire FUV and NUV ranges. We also found that observed and modelled FUV and NUV magnitudes are better reproduced if equal stellar and nebular extinctions in the UV range are adopted.

2. It is found that the infrared luminosity of CSFGs in the observed wavelength range 8 - 1000  $\mu\text{m}$  is nearly equal to the luminosity absorbed at shorter wavelengths  $\leq 1 \mu\text{m}$ , independently of the stellar mass of the galaxy, extinction and the age of the starburst. This indicates that our CSFGs are relatively transparent with small variations of the extinction. There is no evident sign of considerable star formation (SF) located in highly obscured regions, which are not seen in the UV and optical ranges.

3. The slopes  $\beta$  of the SEDs in the UV of our CSFGs vary in the wide range from -2.5 to +1. Most of this spread ( $> 70\%$  by value) is caused by the extinction. Only  $\leq 30\%$  of the spread in  $\beta$  is due to various starburst ages.

4. The log of the intrinsic efficiency of ionising photon production  $\xi$  in our CSFGs varies in a wide range between 24.0 and 25.7 due to the bursting nature of the SF with clear offsets between the CSFGs with high  $\text{EW}(H\beta)$  (young bursts) and with low  $\text{EW}(H\beta)$  (older bursts). Reducing to a zero burst age we eliminate the offset between CSFGs with low and high  $\text{EW}(H\beta)$ s. The reduced values of  $\log \xi_0$  evenly scatter around the value of 25.8, which is close to the value of zero age bursts. However, we argue that for studying the problem of the reionisation of the Universe at redshifts 5 - 10 the canonical value of  $\sim 25.2$  globally may be used assuming

that high-redshift SFGs were formed with a constant rate over a period of several hundred Myr.

## ACKNOWLEDGEMENTS

Funding for the SDSS and SDSS-II was provided by the Alfred P. Sloan Foundation, the Participating Institutions, the National Science Foundation, the U.S. Department of Energy, the National Aeronautics and Space Administration, the Japanese Monbukagakusho, the Max Planck Society, and the Higher Education Funding Council for England. The SDSS was managed by the Astrophysical Research Consortium for the Participating Institutions. Funding for SDSS-III has been provided by the Alfred P. Sloan Foundation, the Participating Institutions, the National Science Foundation, and the U.S. Department of Energy Office of Science. The SDSS-III web site is <http://www.sdss3.org/>. SDSS-III is managed by the Astrophysical Research Consortium for the Participating Institutions of the SDSS-III Collaboration. GALEX is a NASA mission managed by the Jet Propulsion Laboratory. This research has made use of the NASA/IPAC Extragalactic Database (NED) which is operated by the Jet Propulsion Laboratory, California Institute of Technology, under contract with the National Aeronautics and Space Administration.

## REFERENCES

- Alam S. et al., 2015, ApJS, 219, 12  
 Baldwin J. A., Phillips M. M., Terlevich R., 1981, PASP, 93, 5  
 Boquien M. et al., 2012, A&A, 539, A145  
 Bouwens R. J. et al., 2014, ApJ, 793, 115  
 Bouwens R. J. et al., 2015, ApJ, 803, 34  
 Bouwens R. J., Smit R., Labbé I., Franx M., Caruana J., Oesch P., Stefanon M., Rasappu, N., 2016a, ApJ, 831, 176  
 Bouwens R. et al., 2016b, ApJ, 833, 72  
 Calzetti D., 1997, AJ, 113, 162  
 Calzetti D., Kinney A. L., Storchi-Bergmann T., 1994, ApJ, 429, 582  
 Calzetti D., Armus L., Bohlin R. C., Kinney A. L., Koornneef J., Storchi-Bergmann T., 2000, ApJ, 533, 682  
 Cardamone C. et al., 2009, MNRAS, 399, 1191  
 Cardelli J. A., Clayton G. C., Mathis J. S., 1989, ApJ, 345, 245  
 Czerny B., Li J., Loska Z., Szczerba R., 2004, MNRAS, 348, L54  
 Draine B. T., 2003, ApJ, 598, 1017  
 Erb D. K., Steidel C. C., Shapley A. E., Pettini M., Reddy N. A., Adelberger K. L., 2006, ApJ, 647, 128  
 Finkelstein S. L. et al., 2012, ApJ, 756, 164  
 Forrest B. et al., 2016, ApJ, 818, L26  
 Gaskell C. M., Goosmann R. W., Antonucci R. R. J., Whyson D. H., 2004, ApJ, 616, 147  
 Girardi L., Bressan A., Bertelli G. Chiosi C., 2000, A&AS, 141, 371  
 Holden B. P. et al., 2016, ApJ, 820, 73  
 Hunt L. K. et al., 2014, A&A, 561, A49  
 Hurwitz M., Bowyer S., Martin C., 1991, ApJ, 372, 167  
 Izotov Y. I., Thuan T. X., 2011, ApJ, 734, 82

- Izotov Y. I., Thuan T. X., 2016, *MNRAS*, 457, 64
- Izotov Y. I., Thuan T. X., Wilson J. C., 2009, *ApJ*, 703, 1984
- Izotov Y. I., Guseva N. G., Thuan T. X., 2011, *ApJ*, 728, 161
- Izotov Y. I., Guseva N. G., Fricke K. J., Henkel C., 2014a, *A&A*, 561, A33
- Izotov Y. I., Guseva N. G., Fricke K. J., Krügel E., Henkel C., 2014b, *A&A*, 570, A97
- Izotov Y. I., Guseva N. G., Fricke K. J., Henkel C., 2015, *MNRAS*, 451, 2251
- Izotov Y. I., Orlitová I., Schaerer D., Thuan T. X., Verhamme A., Guseva N. G., Worseck G., 2016a, *Nature*, 529, 178
- Izotov Y. I., Schaerer D., Thuan T. X., Worseck G., Guseva N. G., Orlitová I., Verhamme A., 2016b, *MNRAS*, 461, 3683
- Izotov Y. I., Guseva N. G., Fricke K. J., Henkel C., 2016c, *MNRAS*, 462, 4427
- Kashino D. et al., 2013, *ApJ*, 777, L8
- Kauffmann G. et al., 2003, *MNRAS*, 341, 33
- Kong X., Charlot S., Brinchmann J., Fall S. M., 2014, *MNRAS*, 349, 769
- Kurczynski P. et al., 2016, *ApJ*, 793, L5
- Leitherer C. et al., 1999, *ApJS*, 123, 3
- Leitherer C., Ekström S., Meynet G., Schaerer D., Agienko K. B., Levesque E. M., 2014, *ApJS*, 212, 14
- Lejeune T., Buser R., Cuisinier F., 1997, *A&AS*, 125, 229
- Matthee J., Sobral D., Best P., Khostovan A. A., Oteo I., Bouwens R., Röttgering H., 2016, *MNRAS*, 465, 3637
- Meurer G. R., Heckman T. M., Calzetti D., 1999, *ApJ*, 521, 64
- Nakajima K., Ellis R. S., Iwata I., Inoue A. K., Kusakabe H., Ouchi M., Robertson B. E., 2016, *ApJ*, 831, L9
- Pannella M. et al., 2015, *ApJ*, 807, 141
- Pettini M., Kellogg M., Steidel C. C., Dickinson M., Adelberger K. L., Giavalisco M., 1998, *ApJ*, 508, 539
- Planck Collaboration XVI, 2014, *A&A*, 571, A16
- Price S. H. et al., 2014, *ApJ*, 788, 86
- Puglisi A. et al., 2016, *A&A*, 586, A83
- Reddy N. A., Erb D. K., Pettini M., Steidel C. C., Shapley A. E., 2010, *ApJ*, 712, 1070
- Reddy N. et al., 2012, *ApJ*, 744, 154
- Reddy N. et al., 2015, *ApJ*, 806, 259
- Reiter A., Schaerer D., Fosbury R. A. E., 2010, *A&A*, 523, A64
- Rémy-Ruyer A. et al., 2013, *A&A*, 557, A95
- Robertson B. E. et al., 2013, *ApJ*, 768, 71
- Salpeter E. E., 1955, *ApJ*, 121, 161
- Schaerer D., Izotov Y. I., Verhamme A., Orlitová I., Thuan T. X., Worseck G., Guseva N. G., 2016, *A&A*, 591, L8
- Schenker M. A., Ellis R. S., Konidaris N. P., Stark D. P., 2013, *ApJ*, 777, 67
- Schmutz W., Leitherer C., Gruenwald, R., 1992, *PASP*, 104, 1164
- Shivaei I. et al., 2016, *ApJ*, 820, L23
- Stark D. P. et al., 2017, *MNRAS*, 464, 469
- Steidel C. S. et al., 2014, *ApJ*, 795, 165
- Storey P. J., Hummer D. G., 1995, *MNRAS*, 272, 41
- Troncoso P. et al., 2014, *A&A*, 563, A58
- Valentino F. et al., 2015, *ApJ*, 801, 132
- Wang L. et al., 2016, *MNRAS*, 461, 1898
- Wilkins S. M., Feng Y., Di-Matteo T., Croft R., Stanway E. R., Bouwens R. J., Thomas P., 2016, *MNRAS*, 458, L6
- Wright E. L., 2006, *PASP*, 118, 1711

This paper has been typeset from a  $\text{\TeX}$ / $\text{\LaTeX}$  file prepared by the author.